THE ASTROPHYSICAL JOURNAL, 367:493–506, 1991 February 1


# HIGH-RATE ACTIVE GALAXY MONITORING AT THE WISE OBSERVATORY. III. THE BROAD-LINE REGION OF NGC 4151

D. MAOZ,[1] H. NETZER, T. MAZEH, S. BECK, E. ALMOZNINO, E. LEIBOWITZ, N. BROSCH, H. MENDELSON, AND A. LAOR[1]
School of Physics and Astronomy and the Wise Observatory of the Raymond and Beverly Sackler Faculty of Exact Sciences, Tel-Aviv University
*Received 1990 March 12; accepted 1990 July 30*

## ABSTRACT

We present results of our AGN monitoring program for the Seyfert galaxy NGC 4151. The high sampling rate and flux calibration accuracy of our observations allowed us in the first two papers in this series to measure accurately the size of the broad line region (BLR) in two Seyfert galaxies, Mrk 279 and NGC 5548. In the present paper, these features of the observations, coupled with large emission-line variations in NGC 4151 during the monitoring period, give light curves whose quality allows, for the first time, a detailed study of the space and velocity distribution of the BLR gas in an AGN. Through cross-correlation, we find that both H$\alpha$ and H$\beta$ lag the continuum variations by $9 \pm 12$ days. Through Fourier and maximum entropy deconvolutions of the continuum and emission-line light curves, we recover the approximate transfer function of the BLR in this object. We carry out a fitting procedure to the emission-line light curve to investigate the parameter space of the BLR. The latter two analyses suggest that the BLR can best be modeled as either a thick spherical shell or a thin disk viewed nearly edge-on. The ratio of outer to inner radii in these geometries is of order 10, with the inner radius of order several light-days. The line emission of the BLR decreases or is constant with distance from the center. Large regions of parameter space can be significantly excluded. In particular, flat geometries viewed nearly face-on, with line emission increasing with distance from the center, fail to reproduce the observations. The blue and the red wings of the H$\alpha$ and H$\beta$ line profile have an almost identical light curve with little time lag between them. Cross-correlation analysis and simulations significantly rule out pure unidirectional radial motion (either inflow or outflow) of the BLR gas. The consequences of the above findings to our current understanding of AGNs are briefly discussed.

*Subject headings:* galaxies: individual (NGC 4151) — galaxies: nuclei — galaxies: photometry — galaxies: Seyfert

## I. INTRODUCTION

The monitoring of continuum and emission-line variability in active galactic nuclei (AGNs) is gaining increasing application as a method for probing the inner regions of these objects (see Peterson 1988, and references therein). This is currently the only technique that enables a nearly direct determinaton of the size, structure, and dynamics of the broad line region (BLR).

This paper is the third in a series in which we present the results of an intensive AGN monitoring program carried out at the Wise Observatory between 1987 December and 1988 July. The observational setup and data reduction method were described in detail in Paper I of the series (Maoz *et al.* 1990, hereafter Paper I), where results were presented for the Seyfert galaxy Mrk 279. In Paper II (Netzer *et al.* 1990, hereafter Paper II), we presented results for the Seyfert galaxy NGC 5548. The fine temporal sampling and high flux calibration accuracy of our observations allowed, for the first time, an accurate measurement of the lag in the emission-line response to continuum variations. We found H$\alpha$ and H$\beta$ lagged the continuum by 12 days in Mrk 279 and by 7 days in NGC 5548. Through Monte Carlo simulations, we then estimated the characteristic size of the BLR in these AGNs to be 9–15 lt-days and 4–10 lt-days, respectively. The data ruled out at the 95% significance level thin spherical shell-type BLRs larger than 21 lt-days for Mrk 279 and 14 lt-days for NGC 5548, in conflict with the predictions of "standard" photoionization models of AGNs. In this paper we present results for an additional AGN in our sample, NGC 4151.

NGC 4151 is the best studied Seyfert 1 galaxy. A review of work on its variability appears in Peterson (1988). These studies are based mainly on three data sets: Antonucci and Cohen (1983), Ulrich *et al.* (1984) and Clavel *et al.* (1987), and Peterson and Cota (1988). The emerging picture is of a BLR size somewhere between 2 and 20 lt-days. This picture is, however, far from clear. Edelson and Krolik (1988) and Maoz and Netzer (1989) disputed the finding that larger BLRs were significantly ruled out in this object. Peterson and Cota (1988) have also disputed earlier claims by Gaskell and Sparke (1986) that different lines respond with significantly different lags to the continuum; this had been cited as evidence for ionization stratification in the BLR. The controversy stems from the fact that the above data sets are temporally undersampled and/or showed variations which were small compared to the measurement error. Recently, Clavel *et al.* (1991) monitored NGC 4151 intensively with *IUE* during an outburst in late 1988 and found a lag of $4 \pm 3$ days in the C IV $\lambda$1549 and Mg II $\lambda$2798 response to the continuum.

In this paper we present a new data set that considerably improves the situation and enables, for the first time, a detailed look into the inner regions of NGC 4151. In § II, below, we present our data. In § III, four types of analysis are carried out: cross-correlation, to derive the characteristic lag of the lines to the continuum; deconvolution, to recover the BLR transfer function; modeling, to determine the best-fit parameters of the

[1] Present address: Institute for Advanced Study, Princeton.

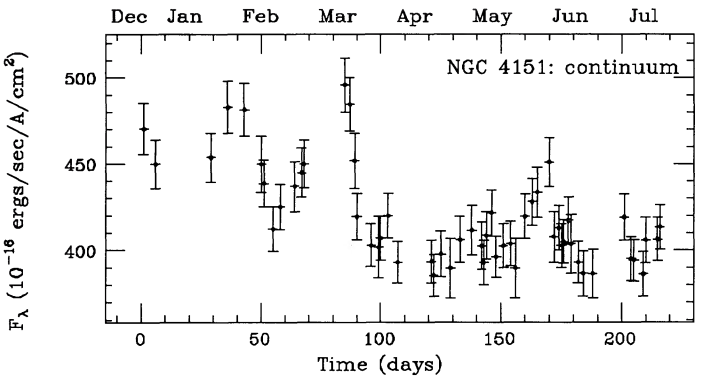


FIG. 1*a*

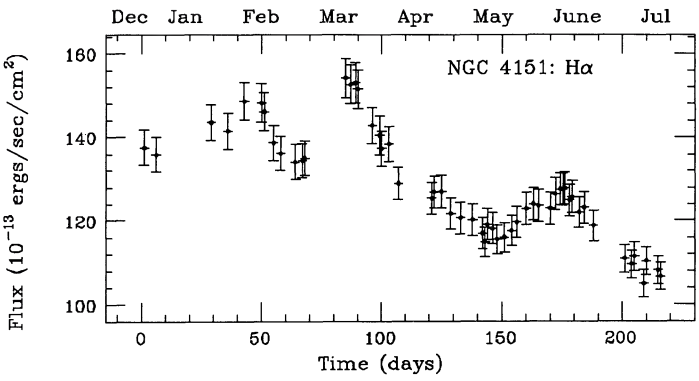


FIG. 1*b*

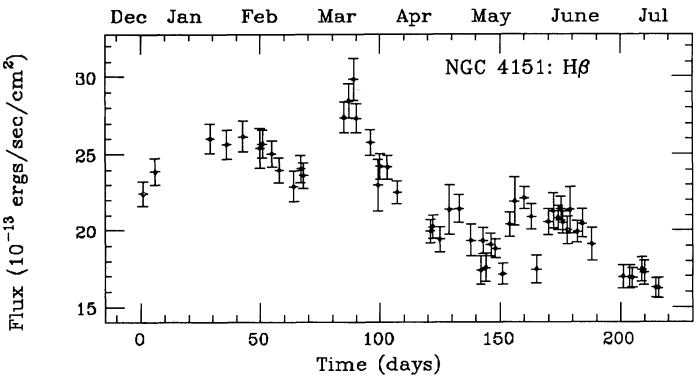


FIG. 1*c*

FIG. 1.—Line and continuum light curves of NGC 4151. (*a*) The 4705–4765 Å continuum. Error bars denote the 1 $\sigma$ uncertainty. (*b*) H$\alpha$. (*c*) H$\beta$.

BLR and the regions of parameter space which can be excluded; and comparison of the blue and red wings of the emission lines, to deduce information on the velocity field of the BLR of NGC 4151. The results are briefly discussed and summarized in § IV.

## II. DATA

A detailed description of the observing procedure and data reduction was given in Papers I and II and will not be repeated here. We will note only those details specific to NGC 4151.

We observed NGC 4151 with the Wise Observatory 1 m telescope on 67 nights during a 216 day period between 1987 December 15 and 1988 July 18. "Star 1" of Penston, Penston, and Sandage (1971) was observed simultaneously through the same slit and served as a comparison standard. In Papers I and II a "quality criterion" was applied to the two consecutive exposures taken each night of each AGN, which required the ratio of the galaxy spectrum to the comparison star spectrum in the two exposures to be identical to within 3%. This was mainly meant to eliminate spectra in which light loss, due to improper positioning and guiding, had occurred. Because of the large angular extent of NGC 4151 and the weakness of the nucleus relative to the stellar continuum, the criterion was relaxed, so that in spectra where the difference between the two exposures was between 3% and 7%, the exposure with the larger galaxy-to-star ratio was taken, assuming this exposure had suffered less from light loss.

Following this procedure acceptable spectra for 55 nights were obtained. The [O III] $\lambda\lambda$4959, 5007 flux in these spectra has a standard deviation of 3%, as expected from the intrinsic accuracy of our observations (see Paper I), indicating that the relaxed quality criterion has not introduced systematically erroneous data. In order to further improve the accuracy of our measurements, we took advantage of the very high signal-to-noise ratio of the data for this object and normalized all spectra to have the same flux in the [O III] $\lambda\lambda$4959, 5007 lines (i.e., a correction of up to a few percent). The Balmer line fluxes we present below are probably, therefore, accurate to *better* than 3%. The same cannot be said of the continuum measurements, since much of the continuum light comes from a more extended area around the nucleus, and some of it may have been lost in spectra passing only the relaxed quality criterion. We therefore estimate a 1 $\sigma$ error of 3% in both the continuum and line measurements, though for the latter this should be regarded as an upper limit.

In its observed faint state, the continuum emission of NGC 4151 is dominated by the stellar component, which, through our aperture, contributes about 80% of the total continuum at 5400 Å (Malkan and Filippenko 1983). Broad H$\alpha$ and H$\beta$ are blended with strong narrow components and forbidden lines. As in Papers I and II, we make no attempt to subtract or deblend any of these features and quote below the total flux in the specified wavelength intervals.

The continuum flux density of NGC 4151 was measured in three wavelength bands (measured in the galaxy's rest frame): 4705–4765 Å, 5065–5125 Å, and 6130–6230 Å. The flux in H$\beta$ was integrated from 4795 to 4915 Å, with the continuum assumed to be a straight line in $F_\lambda$ between the first two bands. H$\alpha$ was integrated from 6410 to 6670 Å, with the continuum extrapolated at constant $F_\lambda$ from the third band. Table 1 gives the results of these measurements. The light curves of the blue continuum band (which is least dominated by the stellar continuum), H$\alpha$, and H$\beta$ are shown in Figure 1. The error bars were computed as in Papers I and II, accounting for the 3% calibration error, the error due to statistical noise, and the propagation of the error in setting the continuum level beneath the lines. For H$\alpha$, the signal is strong enough that the total error is always dominated by the calibration error. In the H$\beta$ light curve, on the other hand, measurements taken during cloudy weather are affected by count statistics and therefore have larger error bars. This explains the "noisier" appearance of the light curve.

## III. ANALYSIS

Figure 1*a* shows that the total continuum of NGC 4151 underwent a general decrease of about 20% amplitude during the period we observed it. From Malkan and Filippenko

TABLE 1

LINE AND CONTINUUM MEASUREMENTS FOR NGC 4151

| DATE (1988) | DAY | 4735 Å CONTINUUM ($10^{-16}$ ergs s$^{-1}$ cm$^{-2}$ Å$^{-1}$) | Hα ($10^{-14}$ ergs s$^{-1}$ cm$^{-2}$) | | | Hβ ($10^{-14}$ ergs s$^{-1}$ cm$^{-2}$) | | |
|---|---|---|---|---|---|---|---|---|
| | | | Total | Red | Blue | Total | Red | Blue |
| Dec 15[a] | 1[b] | 470 ± 15 | 1375 | 730 | 649 | 224 ± 8 | 112 | 111 |
| Dec 20[a] | 6 | 450 ± 14 | 1358 | 730 | 630 | 238 ± 8 | 114 | 124 |
| Jan 13 | 29 | 453 ± 14 | 1435 | ... | ... | 260 ± 9 | ... | ... |
| Jan 20 | 36 | 483 ± 15 | 1414 | 754 | 661 | 256 ± 9 | 124 | 131 |
| Jan 27 | 43 | 481 ± 15 | 1486 | 778 | 709 | 261 ± 9 | 120 | 140 |
| Feb 3 | 50 | 450 ± 16 | 1482 | ... | ... | 253 ± 12 | ... | ... |
| Feb 4 | 51 | 439 ± 14 | 1461 | 746 | 716 | 256 ± 8 | 116 | 139 |
| Feb 8 | 55 | 412 ± 13 | 1385 | 700 | 692 | 250 ± 8 | 114 | 136 |
| Feb 11 | 58 | 425 ± 13 | 1361 | 715 | 646 | 239 ± 7 | 106 | 133 |
| Feb 17 | 64 | 437 ± 14 | 1340 | 719 | 617 | 228 ± 9 | 112 | 117 |
| Feb 20 | 67 | 445 ± 14 | 1343 | 714 | 629 | 240 ± 8 | 119 | 120 |
| Feb 21 | 68 | 450 ± 14 | 1349 | ... | ... | 235 ± 8 | 115 | 121 |
| Mar 9 | 85 | 496 ± 16 | 1541 | 813 | 726 | 273 ± 10 | 142 | 131 |
| Mar 11 | 87 | 484 ± 16 | 1526 | 822 | 705 | 284 ± 10 | 133 | 150 |
| Mar 13 | 89 | 452 ± 16 | 1530 | 809 | 717 | 298 ± 13 | 152 | 145 |
| Mar 14 | 90 | 419 ± 13 | 1515 | 801 | 714 | 273 ± 9 | 137 | 145 |
| Mar 20 | 96 | 403 ± 12 | 1428 | ... | ... | 257 ± 8 | ... | ... |
| Mar 23 | 99 | 402 ± 18 | 1404 | 747 | 652 | 229 ± 16 | 115 | 114 |
| Mar 24 | 100 | 407 ± 13 | 1372 | 731 | 639 | 241 ± 8 | 120 | 121 |
| Mar 27 | 103 | 420 ± 13 | 1383 | 729 | 650 | 241 ± 7 | 112 | 128 |
| Mar 31 | 107 | 393 ± 12 | 1288 | 678 | 605 | 224 ± 7 | ... | ... |
| Apr 14 | 121 | 393 ± 12 | 1252 | 660 | 593 | 199 ± 7 | 89 | 110 |
| Apr 15 | 122 | 385 ± 12 | 1267 | 681 | 585 | 202 ± 7 | 83 | 119 |
| Apr 18 | 125 | 398 ± 13 | 1269 | 678 | 589 | 194 ± 8 | 89 | 104 |
| Apr 22 | 129 | 390 ± 17 | 1216 | 655 | 560 | 213 ± 16 | 97 | 115 |
| Apr 26 | 133 | 406 ± 13 | 1206 | 642 | 563 | 213 ± 9 | 110 | 103 |
| May 1 | 138 | 411 ± 14 | 2101 | 654 | 547 | 193 ± 10 | 95 | 98 |
| May 5 | 142 | 402 ± 14 | 1169 | 635 | 532 | 173 ± 9 | 85 | 88 |
| May 6 | 143 | 393 ± 13 | 1148 | 622 | 526 | 193 ± 8 | 92 | 101 |
| May 7 | 144 | 408 ± 14 | 1190 | 652 | 538 | 175 ± 9 | 84 | 91 |
| May 9 | 146 | 421 ± 13 | 1181 | 636 | 546 | 190 ± 7 | 86 | 104 |
| May 11 | 148 | 396 ± 12 | 1154 | 642 | 516 | 188 ± 6 | 84 | 103 |
| May 14 | 151 | 402 ± 13 | 1159 | 599 | 559 | 171 ± 6 | 84 | 86 |
| May 17 | 154 | 404 ± 13 | 1175 | 654 | 522 | 204 ± 8 | 100 | 103 |
| May 19 | 156 | 390 ± 17 | 1196 | 634 | 565 | 219 ± 15 | 106 | 112 |
| May 23 | 160 | 419 ± 13 | 1228 | 663 | 569 | 221 ± 7 | 103 | 117 |
| May 26 | 163 | 428 ± 14 | 1239 | 660 | 581 | 208 ± 8 | 95 | 113 |
| May 28 | 165 | 433 ± 15 | 1235 | 649 | 590 | 174 ± 9 | 83 | 91 |
| Jun 2 | 170 | 451 ± 14 | 1229 | 648 | 583 | 205 ± 8 | 89 | 117 |
| Jun 4 | 172 | 408 ± 15 | 1264 | 680 | 584 | 212 ± 11 | 94 | 118 |
| Jun 6 | 174 | 413 ± 13 | 1275 | 673 | 604 | 208 ± 7 | 98 | 109 |
| Jun 7 | 175 | 403 ± 13 | 1275 | ... | ... | 214 ± 7 | ... | ... |
| Jun 8 | 176 | 405 ± 13 | 1278 | 679 | 603 | 205 ± 7 | 94 | 110 |
| Jun 10 | 178 | 417 ± 14 | 1248 | 661 | 591 | 200 ± 8 | 95 | 104 |
| Jun 11 | 179 | 404 ± 17 | 1257 | ... | ... | 213 ± 15 | ... | ... |
| Jun 14 | 182 | 393 ± 12 | 1220 | 660 | 559 | 199 ± 6 | 86 | 112 |
| Jun 16 | 184 | 386 ± 13 | 1231 | 653 | 582 | 204 ± 9 | 92 | 111 |
| Jun 20 | 188 | 386 ± 14 | 1188 | ... | ... | 191 ± 10 | ... | ... |
| Jul 3 | 201 | 419 ± 14 | 1108 | 600 | 510 | 169 ± 7 | 77 | 92 |
| Jul 6 | 204 | 395 ± 13 | 1095 | 587 | 510 | 169 ± 7 | 82 | 86 |
| Jul 7 | 205 | 394 ± 12 | 1113 | 609 | 501 | 169 ± 6 | 77 | 91 |
| Jul 11 | 209 | 386 ± 13 | 1049 | 576 | 472 | 174 ± 8 | 93 | 81 |
| Jul 12 | 210 | 406 ± 13 | 1103 | 614 | 490 | 172 ± 8 | 80 | 91 |
| Jul 17 | 215 | 406 ± 13 | 1080 | 566 | 516 | 162 ± 6 | 77 | 84 |
| Jul 18 | 216 | 413 ± 13 | 1065 | 561 | 503 | 162 ± 6 | 75 | 87 |

NOTE.—1 $\sigma$ errors in the total Hα flux are 3%. Epochs without red/blue wing data were not suitable for this measurement (see text). See text for details of red/blue wing measurement errors.

[a] 1987.

[b] JD 2,447,145.

(1983), we find that the stellar contribution through our aperture is $3.3 \times 10^{-14}$ ergs s$^{-1}$ Å$^{-1}$ cm$^{-2}$ with a quoted uncertainty of 10%–20%. The observed variation therefore indicates a significant decline, by at least a factor of 2, of the already weak nonstellar continuum. Superposed on this trend are three 'bumps." The first of these is badly sampled. The second, and most notable, bump consists of a possibly gradual rise interrupted by a large gap in the sampling, followed by a very steep, but well-sampled fall. The third bump in the light curve appears to have a similar structure and is well sampled, but has a smaller amplitude.

During one of the gaps in our continuum light curve,

between days 107 and 121, Solomos *et al.* (1990) monitored NGC 4151 photometrically. Their data, which consist of seven observations between days 109 and 128, show that the 5672 Å continuum was constant to within an uncertainty of a few percent. Our continuum measurements on days 107 and 121 are identical, so a linear interpolation over this gap will be well justified.

The light curves of Hα and Hβ in Figures 1*b* and 1*c* reflect both the decreasing trend and the three bumps in the continuum light curve. The peaks of the bumps, however, seem visibly delayed and, rather than falling steeply like the bumps in the continuum light curve, decrease very gradually.

The mean sampling interval in these data is less than 4 days, which is short compared to the typical time scale of the variations (28 days, as determined from the FWHM of the continuum autocorrelation function). The total extent of the time series (216 days) is long compared to the variation time scale, thus allowing us to discern several separate "events." The ratio of maximum to minimum flux is about 1.25 in the continuum and 1.5 in the lines, so that the amplitude of the variations is large compared to the measurement errors. Excepting perhaps the recently obtained data from the *IUE* project of monitoring NGC 5548 (Clavel *et al.* 1990), this is therefore the best data set of its kind, in terms of the wealth of detail revealed in the light curves. In view of this, we carry out a more sophisticated analysis of the data than has been attempted before, with the purpose of extracting from them the maximum available information concerning the BLR of NGC 4151. As in Papers I and II, we cross-correlate the light curves to derive a characteristic size for the BLR (§ III*a*). Following the theoretical work of Blandford and McKee (1982), we Fourier-deconvolve the light curves to recover the transfer function of the BLR, from which its geometric characteristics can be estimated (§ III*b*). We also recover the BLR transfer function using maximum entropy deconvolution (§ III*c*). We fit models to the light curves to find the best parameters for the BLR structure (§ III*d*). Finally, we study the velocity field of the BLR as reflected in the variations of the blue and red wings of the emission lines (§ III*e*).

### *a) Cross-Correlation*

The cross-correlation functions of Hα and Hβ versus the 4735 Å continuum are shown in Figure 2*a*. Both are very similar and have sharp peaks of 0.84 and 0.82, respectively, at a lag of 9 days. (Cross-correlation peaks are determined here and in the rest of the paper through a parabolic fit to the upper-third of the cross-correlation function). The similarity of the two emission-line light curves can also be seen from the cross-correlation function of Hβ versus. Hα, shown in Figure 2*b*, which is very symmetric and highly peaked (0.95) at zero-lag. At face value, the results therefore imply a characteristic size of 9 lt-days for the BLR of NGC 4151. As we will, however, show below and in § III*d*, the characteristic size may be larger for certain BLR geometries.

We have also calculated the discrete correlation functions (Edelson and Krolik 1988) for these data and find that they follow the cross-correlation functions of Figures 2*a* and 2*b* closely. From this we conclude that the cross-correlation results have not been affected by artificial interpolated data or correlated errors.

To evaluate the significance of the cross-correlation results and their uncertainty, we carried out Monte-Carlo simulations, as described by Maoz and Netzer (1989), and in Papers I and II. A model light curve for the continuum of NGC 4151 was created by linearly interpolating the observed continuum light curve. The probability of obtaining the above cross-correlation results was found by sampling artificial data sets calculated for a variety of spherical BLR geometries. The reader is referred to the above papers for further details on the simulations.

Figure 3 shows the regions of the parameter space of inner and outer BLR radius which, according to the simulations, can be ruled out at the 95% significance level or better. It indicates that the cross-correlation results allow "thin" spherical geometries (i.e., with $R_{in} \approx R_{out}$) for only a narrow range of BLR radii, between 7 and 11 lt-days. On the other hand, a large variety of "thick" geometries is allowed, but these are constrained to have an inner radius of less than about 8 lt-days

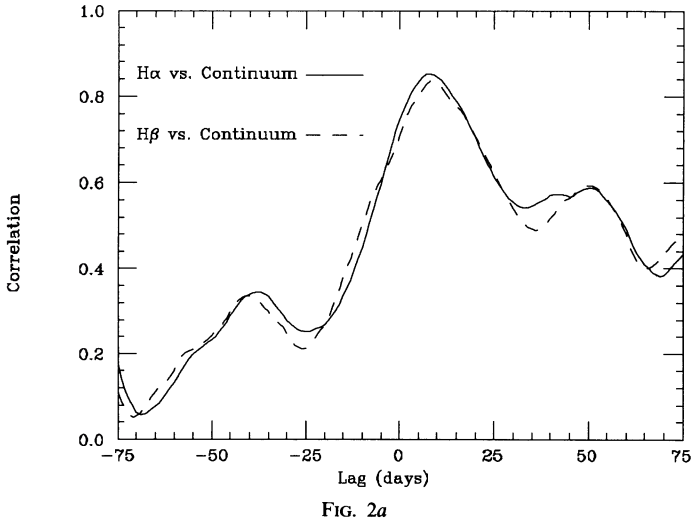


FIG. 2*a*

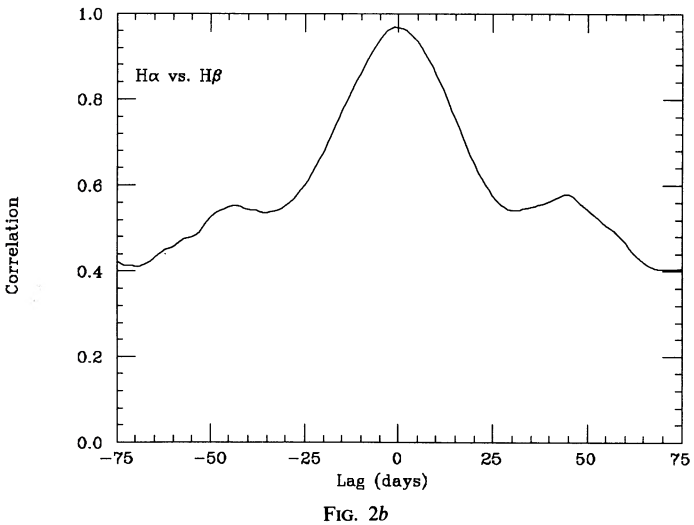


FIG. 2*b*

FIG. 2.—(*a*) The cross-correlation functions of Hα vs. the 4705–4765 Å continuum (*solid line*) and Hβ vs. this continuum (*dashed line*). (*b*) Cross-correlation of Hα vs. Hβ.

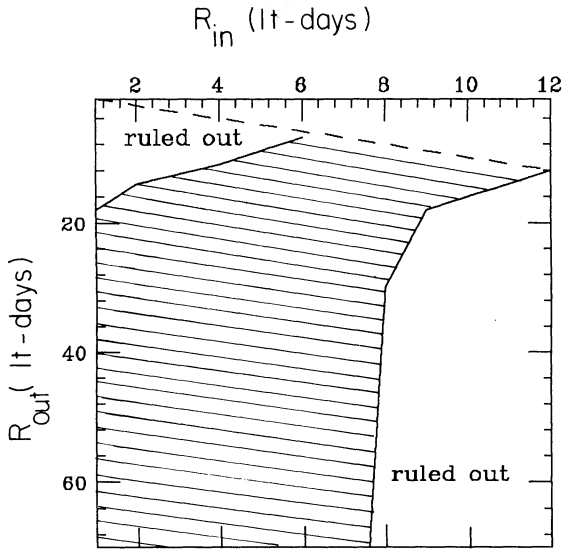


FIG. 3.—The parameter space of inner and outer BLR radius ($R_{in}$ and $R_{out}$) of NGC 4151. Regions ruled out at better than 95% significance level by analysis of the cross-correlation results are indicated. The allowed area is hatched. The dashed line is $R_{in} = R_{out}$; the region above it ($R_{in} > R_{out}$) is meaningless.

if the observed cross-correlation peak is to be reproduced with better than 5% probability. We note, however, that this relates to only one possible type of BLR geometry (spherical). Also, the line response of each model is calculated under the assumption of constant line emission per shell of constant thickness $dr$, an assumption also used in Papers I and II. A more exhaustive investigation of parameter space, in terms of both geometry type and radial dependence of emissivity, will be presented in § III*d*, below.

As explained in the papers cited above, the simulations can also yield an estimate of the equivalent of the 1 $\sigma$ uncertainty (i.e., the 68% probability range) in our 9 day lag result, if one assumes a certain type of BLR geometry. For example, for the simplest possible geometry, a thin spherical shell, of radius 9 lt-days, there is a 79% probability of obtaining a cross-correlation peak at a lag of $9 \pm 1$ days, and 94% at $9 \pm 2$ days. However, as we show in the more sophisticated analysis below, a thin shell geometry is probably a poor approximation for the BLR of NGC 4151. For a thick spherical BLR geometry, with inner and outer radii of 1 and 40 lt-days, respectively, there is a 70% probability of obtaining the peak at $8 \pm 2$ days, and 92% at $8 \pm 3$ days. These numbers can therefore be viewed as an estimate of the uncertainty in the lag of the cross-correlation function.

We note that due to the uncertainty regarding the stellar contribution to the continuum and the narrow component to the lines, we cannot say whether the variability amplitude of the nonstellar continuum is much larger than, or comparable to, that of the broad emission lines; taking the lower limit for the stellar contribution from Malkan and Filippenko (1983) leads to a factor of 2 variation of the nonstellar continuum, while taking the upper limit would indicate the continuum varied by a much larger factor. Considering the narrow contribution to the line flux (e.g., Boksenberg *et al.* 1975), the broad-line flux varied by a factor of 1.5–2. If indeed the amplitude of the line variations is much smaller than that of the nonstellar continuum, this could indicate that only the variable component of the lines is coming from a 9 lt-day BLR, while some of the line flux is coming from a separate BLR which is much larger. As the total line flux does, however, decrease during the monitoring period by a factor of 1.5–2, even if the nonstellar continuum decrease is very large, at least one-half of the line-emitting gas is in the 9 lt-day BLR.

### *b) Fourier Deconvolution*

As mentioned above, the detailed structure visible in the light curves suggests that additional information, beyond the characteristic lag between the lines and continuum, can be extracted from the data. We attempt, therefore, to apply the "reverberation mapping" formalism of Blandford and McKee (1982) to our data, with the purpose of deriving the geometric structure of the BLR of NGC 4151. Since this is the first time this technique is applied to real data, we repeat here its main points.

Designate $C(t)$ and $L(t)$ as the continuum and emission line light curves, respectively, at time $t$. Assuming only that (1) the observed optical continuum flux is proportional to the ionizing flux "seen" by the BLR; (2) the flux in emission lines is reprocessed ionizing continuum energy; (3) the flux in the emission line observed is linearly dependent on the continuum flux; and (4) the recombination time scale is much shorter than the light travel time across the BLR and the dynamical time scale is much longer than the time span of the data; then $L(t)$ is the convolution of $C(t)$ with a "transfer function" $\Psi(t)$:

$$L(t) = \int_{-\infty}^{\infty} C(\tau)\Psi(t - \tau)d\tau \, . \tag{1}$$

As can be seen from this equation, $\Psi(t)$, in appropriate units, is the line flux that would be observed following a short continuum flash (a $\delta$-function, at $t = 0$). All the information on the BLR is contained in the transfer function $\Psi$ (sometimes also called the "response function"). It can be recovered from the data by applying the convolution theorem

$$\tilde{\Psi}(\omega) = \frac{\tilde{L}(\omega)}{\tilde{C}(\omega)} \, , \tag{2}$$

where $\tilde{L}(\omega)$ is the Fourier transform of $L(t)$, etc., and then transforming $\tilde{\Psi}(\omega)$ back to the time domain.

Before describing the actual application of the process, we illustrate it in a simulation shown in Figure 4. A synthetic continuum light curve (Fig. 4*a*), obtained by spline interpolating the observed NGC 4151 continuum light curve, is convolved with the transfer function (Fig. 4*b*) characteristic of a spherical BLR geometry with inner and outer radii of 5 and 20 lt-days, respectively. (A more detailed discussion of the transfer functions of various BLR geometries is given below). This gives a synthetic emission line light curve (Fig. 4*c*). These are then deconvolved to recover the transfer function (Fig. 4*d*). If, however, the synthetic light curves are discretely sampled at random at 55 points (as our data set is), interpolated to 1 day intervals, and then deconvolved, the recovered transfer function is noticeably deteriorated, though still recognizable (Fig. 4*e*). Adding a "measurement error" to each point will make the recovered transfer function even noisier (not shown in Fig. 4). Note in Figure 4*d* that, even without the discrete sampling and the measurement error, the exact transfer function cannot be recovered because of the finite sampling window, which introduces some noise. This is a fundamental problem of Fourier techniques, which can be dealt with by using nonlinear

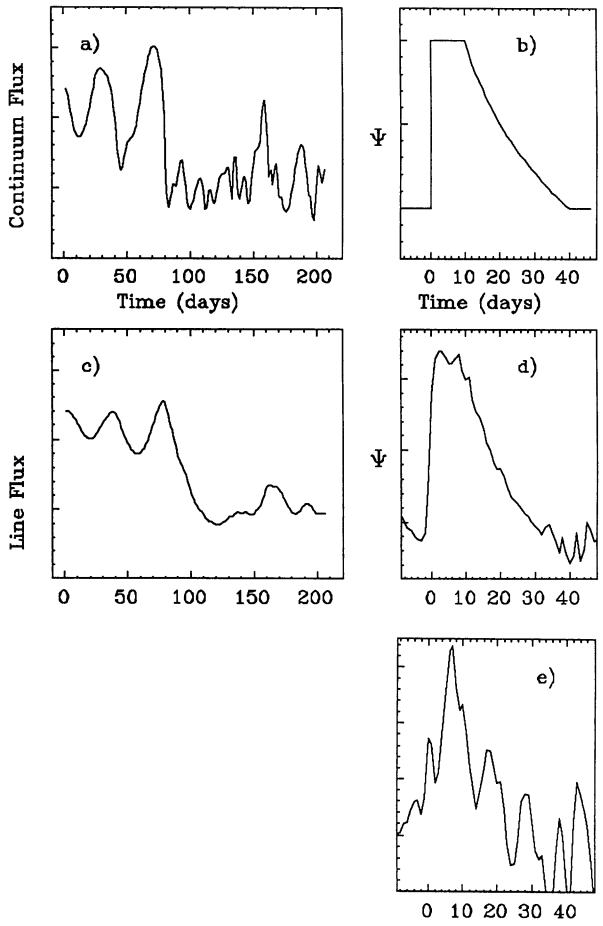


FIG. 4.—Illustration of the Fourier deconvolution technique: A synthetic continuum light curve (*a*) is convolved with the transfer function (*b*) of a spherical BLR geometry of inner and outer radii of 5 and 20 lt-days, respectively, to obtain a synthetic emission line light curve (*c*). The line and continuum light curves are deconvolved to recover the transfer function (*d*). If, however, the light curves are sampled at random at only 55 points, linearly interpolated, and then deconvolved, then the recovered transfer function (*e*) is considerably deteriorated, though still recognizable.

deconvolution methods. One such method, maximum entropy deconvolution, will be used in § III*c*, below.

Fourier-transforming the data for NGC 4151 is not straightforward since they span a finite and relatively short time interval and are unevenly sampled. After experimenting with various procedures, we have arrived at the following one, which we believe is optimal for this data set: The Hα and continuum light curves were linearly interpolated to one day intervals, which are the shortest occurring in the actual data. The mean was subtracted from each light curve and the ends tapered by multiplying them by a cosine bell. The light curves were then Fourier-transformed and their complex Fourier amplitudes divided according to equation (2). $\tilde{\Psi}(\omega)$ was optimally filtered (e.g., Press *et al.* 1986) before transforming it back to the time domain. Figure 5 shows two examples of the resulting $\Psi(t)$ obtained by applying such filters with somewhat different cutoff frequencies.

The overall structure of the transfer function can best be seen in the more strongly filtered function (Fig. 5, *solid line*), where a signal is discernible between approximately 0 and 20 days. In the less filtered function (Fig. 5, *dashed line*), a sharp rise to the maximum level at zero days lag seems to be present,

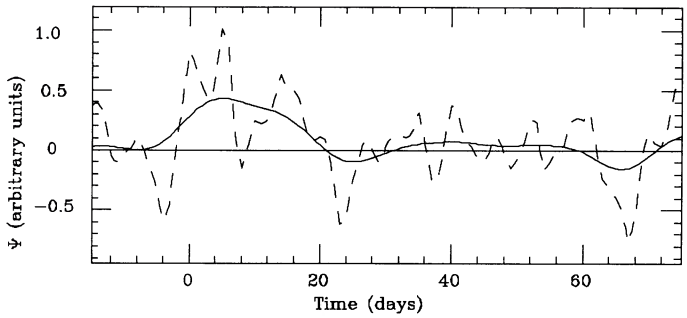


FIG. 5.—The Hα transfer function for NGC 4151, recovered through Fourier deconvolution. The two lines correspond to the filtering of the signal with two different cutoff frequencies.

through this is by no means certain. Note that the gradual rise at negative lag in the strongly filtered function is not a violation of causality in the BLR; the transfer function cannot rise abruptly after the high frequencies have been filtered out of its Fourier spectrum.

We conclude that the Hα response to variations in the continuum is immediate, or nearly so, that it continues, possibly at a constant level, until 10–15 days lag, and that it then declines until it merges with the noise at a lag of about 20 days. The types of geometry which can give such a transfer function are discussed below.

The line emission $dI(r)$ from the BLR at a distance $r$ from the center is

$$dI(r) = \epsilon(r)N(r)4\pi r^2\, dr\ ,$$

where $N(r)$ is the space density of line emitting objects, and $\epsilon(r)$ is the emission of a single line emitting object at distance $r$ (e.g., Rees, Netzer, and Ferland 1989; Scoville and Norman 1988; Kazanas 1989). In optically thick photoionization models (the only situation considered in this paper), all ionizing radiation impinging on a line-emitting object is absorbed by it. $\epsilon(r)$ is then simply proportional to the fractional cross-sectional area $\sigma(r)$ occupied by the emitting object: $\epsilon(r) \propto \sigma(r)/4\pi r^2$. The line emission at a distance $r$ from the center then depends only on the differential covering factor $dC(r)$, defined as the fraction of the sky, as viewed from the central source, covered by the line emitting objects at radii $r$ to $r + dr$: $dI(r) \propto dC(r) = N(r)\sigma(r)dr$. In order keep our discussion as general as possible, rather than oriented toward a certain model, we find it convenient to deal with $dC(r)$. Our results can then be used to constrain the parameters of the various models. Accordingly, we parametrize $dC(r)$ to have a power-law dependence on radius, $dC(r) \propto r^{\alpha}\, dr$, between inner and outer radii $R_{\rm in}$ and $R_{\rm out}$.

The transfer function of a thin spherical shell of radius $r$ is a constant "boxcar"-shaped pulse lasting from $t = 0$ until $t = 2r/c$, where $c$ is the speed of light, and intensity proportional to $1/2r$. To calculate the transfer function of a thick spherical shell, we integrate this transfer function over all radii, weighting the contribution at each radius according to the differential covering factor:

$$\Psi(t) \propto \int \frac{dC(r)}{r}\ . \qquad (3)$$

For any spherical geometry, regardless of $\alpha$, the integral in equation (3) is a constant in time between $t = 0$ and $t = 2R_{\rm in}/c$, and a declining function of time between $t = 2R_{\rm in}/c$ and $t =$

$2R_{out}/c$, after which $\Psi(t)$ returns to zero:

$$\Psi(t) = \text{const}, \qquad 0 < t \le 2R_{in}/c$$
$$= \text{const} \times \int_{r=ct/2}^{R_{out}} r^{\alpha-1}\, dr, \qquad 2R_{in}/c \le t \le 2R_{out}/c$$
$$= 0, \qquad \text{otherwise}.$$

Figure 6*a* shows the transfer functions of a spherical shell of inner radius 10 lt-days and outer radius 20 lt-days with $\alpha$ ranging from $-2$ (emission sharply peaked near $R_{in}$), through 0 (constant emission per shell of thickness $dr$), to 2 (emission weighted toward $R_{out}$).

The transfer function of a ring of radius $r$ and inclination angle $i$ to the line of sight is

$$\Psi(t) = \text{const.} \times r^{-1}\left[\sin^2 i - \left(1 - \frac{ct}{r}\right)^2\right]^{-1/2},$$
$$\frac{r}{c}(1 - \sin i) \le t \le \frac{r}{c}(1 + \sin i)$$
$$\Psi(t) = 0, \quad \text{otherwise}.$$

To obtain the transfer function of a thin disk we integrate over rings, again weighting each ring using $dC(r)$, obtaining (see also Blandford and McKee 1982):

$$\Psi(t) \propto t^{\alpha} \int_{\arccos\{\min[1,\,(1-ct/R_{out})/\sin i]\}}^{\arccos\{\max[-1,\,(1-ct/R_{in})/\sin i]\}} d\phi (1 - \sin i \cos\phi)^{-(\alpha+1)},$$

for $R_{in}(1 - \sin i)/c < t < R_{out}(1 + \sin i)/c$, and 0 otherwise.

The term $dC(r)$ can include a dependence of disk thickness $h(r)$ on radius if we reexpress it in this case as $dC(r) = drN(r)\sigma(r)h(r)/r$. Disk transfer functions generally have a time interval $R_{in}(1 - \sin i)/c$, prior to which $\Psi = 0$. This results from the light travel time from the central source to the part of the inner edge of the disk nearest to the observer. Disk transfer functions also often have a double-peaked structure, although this is not the case for some combinations of $R_{in}$, $R_{out}$, and sin $i$. Blandford and McKee (1982) show the transfer functions of a certain disk model seen at different inclination angles. We show in Figure 6*b* the transfer functions for a disk inclined at 45° to the line of sight and of inner radius 10 lt-days and outer radius 20 lt-days, again for a range of radial dependences of $dC(r)$.

Returning to the observed transfer function of NGC 4151 (Fig. 5), we see that it is consistent with that of a spherical geometry, in terms of the possible fast rise to the maximum level and the plateau following it. A rough estimate of the parameters, from examination of Figure 5, then yields $R_{in} \approx 5$ lt-days and $R_{out} \ge 10$ lt-days. On the other hand, the observed transfer function can also be consistent with a disk geometry for some combinations of parameters; e.g., disks viewed near edge-on can have a transfer function with a sharp rise to maximum followed by a gradual decline. It seems, however, that the data are only marginally adequate to be deconvolved using Fourier methods and do not allow a direct determination of the BLR structure from the transfer function. A more sophisticated deconvolution, using the maximum entropy method, will be applied to the data in § III*c*, below. Nevertheless, the signal in the transfer function can be improved using data that will be obtained in the future for this object; as opposed to light curves and cross-correlation functions which contain information on the temporal behavior of the lines and continuum during a specific period, the transfer function is only characteristic of the BLR geometry. Transfer functions obtained in the future can therefore be averaged with the one obtained here.

### *c) Maximum Entropy Deconvolution*

In the previous subsection we attempted to deduce the transfer function of the BLR of NGC 4151 by a method making minimal assumptions (Fourier deconvolution). In this subsection we recover the transfer function by a second method, maximum entropy deconvolution, which allows implementing some *a priori* assumptions about the transfer function.

Maximum entropy deconvolution is recently finding widespread application in astronomy, mostly in problems of image reconstruction (see Narayan and Nityananda 1986, for a review). In such problems, the method is used to deconvolve an observed image from a known point spread function to recover the undistorted image. Its advantage over Fourier methods is in that it enforces the assumption that the recovered image is everywhere positive, thus avoiding the ringing and overshooting to negative intensities characteristic of Fourier methods. The method also allows implementing further *a priori* assumptions.

In the present problem, we wish to deconvolve the observed emission-line light curve from the continuum light curve to recover the transfer function. The difference between this and the image reconstruction problem is that both light curves are unevenly sampled, and the continuum light curve is corrupted by noise, and thus not well known like the point spread function in the image reconstruction problem. In order to carry out the method, we linearly interpolate the observed light curve to 1 day intervals, as in the previous subsections. The uncertainty

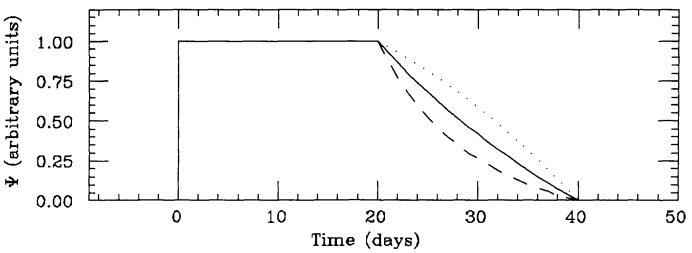


FIG. 6*a*

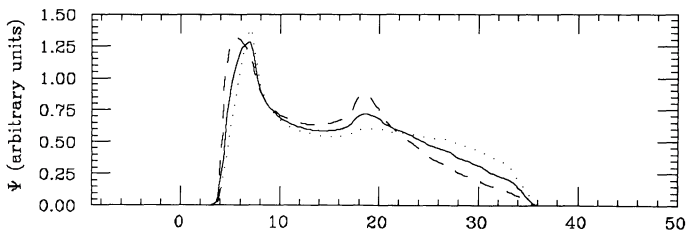


FIG. 6*b*

FIG. 6.—Transfer functions of simple geometries. (*a*) Transfer functions of spherical geometries of inner radius 10 lt-days and outer radius 20 lt-days, with emission parameter $\alpha$ of $-2$ (*dashed line*), 0 (*solid line*), and 2 (*dotted line*). (*b*) Transfer functions of disk geometries inclined by 45° to the line of sight, and inner and outer radii and $\alpha$ as in (*a*).

in the continuum light curve will result in some uncertainty in the results of the method.

The positivity assumption of the maximum entropy method ensures that the recovered transfer function is always positive, or zero, as indeed would be the case for an optically thick BLR responding linearly to continuum variations. We further assume the transfer function is 0 at negative lags, meaning causality is enforced. Finally, we assume that the transfer function is 0 beyond time $t = \frac{2}{3}T$, where $T$ is the time span of the data. This is necessary since, as in cross-correlation, progressively less information is contained in the data regarding larger lags. (The same is often done in the image reconstuction application, where the method is restricted to concentrate on a certain region, outside of which it is constrained to be 0; see Narayan and Nityananda 1986).

To implement the method, we use the recursive algorithm of Willingale (1981), also described in convolution form by Lester, Harvey, and Joy (1986), and slightly modified by us to suit the present application:

$$\mathbf{\Psi}^{i+1} = \beta\gamma \exp\left[\lambda \boldsymbol{C} \otimes (\boldsymbol{L} - \boldsymbol{C} * \mathbf{\Psi}^i)\right] + \beta(1-\gamma)\mathbf{\Psi}^i . \quad (4)$$

$\boldsymbol{C}$ and $\boldsymbol{L}$ are the continuum and line light curves, with the boldfaced characters marking them as vectors. {For example: $\boldsymbol{L} \equiv [L(t_1), L(t_2), \ldots L(t_n)]$.} $\mathbf{\Psi}^i$ is the transfer function after the $i$th iteration. The operator * denotes a convolution, and $\otimes$ a cross-correlation. $\lambda$ is a "sharpness" parameter which is adjusted so that the $\chi^2$ per degree of freedom between the observed emission line light curve, $\boldsymbol{L}$, and the model light curve, $\boldsymbol{C} * \mathbf{\Psi}$, will be of order 1. $\gamma$ is some number between 0 and 1, chosen to ensure that the algorithm converges to a stable solution. $\beta$ is a normalization factor.

The first guess for the transfer function, $\mathbf{\Psi}^1$, is taken to be some arbitrary function, and the algorithm is repeatedly applied until $\mathbf{\Psi}^i$ changes negligibly between iterations. We find the solution is insensitive to the first guess for $\mathbf{\Psi}^1$. The procedure is repeated for different values of $\lambda$ until a solution for $\mathbf{\Psi}$ satisfying the $\chi^2$ criterion is obtained.

Figure 7 shows the transfer function recovered using the maximum entropy method. Figure 8 shows, superposed on the Hα measurements, the model emission line light curve obtained by convolving this transfer function with the continuum light curve.

The transfer function in Figure 7 has a sharp maximum at $t = 0$, followed by steep decline to near zero-level at $t \approx 35$ days. The spike at $t = 0$ (rather than, e.g., the plateau characteristic of spherical geometries with $R_{\rm in} > 0$) could very possibly be an artifact of the method, which has a tendency to produce such sharp features. Similarly, the steepness of the decline is somewhat dependent on the exact value of the $\lambda$ parameter used. The transfer function also has considerable power in an extended "emission" up to $t \approx 120$ days. As can be seen in Figure 8, this transfer function can reproduce the observed emission line light curve remarkably well.

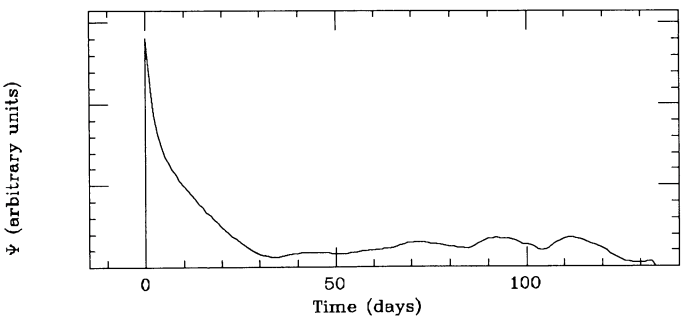


FIG. 7.—The Hα transfer function for NGC 4151 recovered using maximum entropy deconvolution.

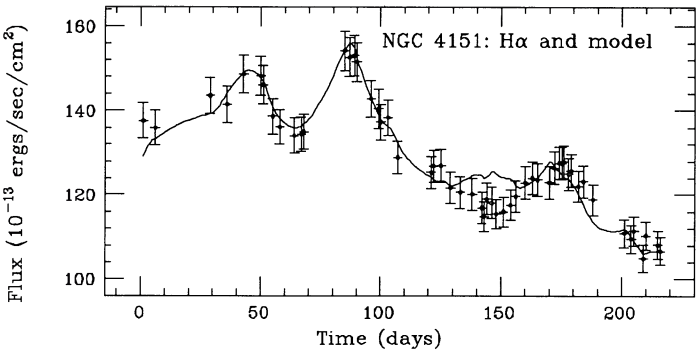


FIG. 8.—Model emission line light curve obtained by convolving the transfer function obtained from maximum entropy deconvolution (Fig. 7) with the interpolated observed continuum light curve. The observed Hα measurements are superposed.

Clearly, the transfer function in Figure 7 would not arise from one of the simple geometries considered in § III*b*; apart from the extended structure at long lags, the decline from $t = 0$ has a functional form more complicated than the power laws resulting from the constant $\alpha$ models of § III*b*. Nevertheless, its general form is similar to that of some of the functions found there, in terms of the maximum at or near $t = 0$. A BLR geometry which could give this transfer function is a thick spherical geometry of small inner radius, and outer radius of $\sim 15$ lt-days, together with a more extended component of size $\sim 60$ lt-days. As mentioned in § III*b*, a disk geometry viewed nearly edge-on could also give a similar form.

The transfer function in Figure 7 thus exemplifies the possibility that the geometry of the BLR may not be the simplest which comes to mind. It should be remembered, however, that the continuum light curve is corrupted by measurement and interpolation errors, which could distort the transfer function we derived. This possibility is further investigated in § III*d*, below.

### *d) Light Curve Modeling*

In this section, we follow the alternative program suggested by Blandford and McKee (1982): In an attempt to find the best-fit parameters of the BLR, and to evaluate the relevance of various geometries, we fit models to the observed emission-line light curve. This fit is done by convolving the linearly interpolated observed continuum light curve with the transfer function of a specific geometry. We run a grid of models with the type of geometry (spherical, or flat with a given inclination), $\alpha$, $R_{\rm in}$, and $R_{\rm out}$ as free parameters. For each model the calculated light curve is normalized to have the same mean and standard deviation as the observed Hα light curve (equivalent to the requirement that the time integrated intensity of the model equal that of the data), and the $\chi^2$ between the observed and the synthetic light curve calculated. In this fitting procedure, the first 28 days in the calculated and observed Hα light curves are excluded, since they include the reponse to continuum variations which occured *before* the monitoring began, and on which we therefore have no information. (Apart from the consideration that the third data point is on day 29, the choice of

28 days is somewhat arbitrary, and is guided by the fact that the charactristic lag is 9 days, so that previous continuum events should have little effect after 28 days.) We have also found it necessary to exclude the last 20 days from the fit for the following reason: The continuum measurement at day 201 is unusually high, compared with its neighboring points, and is preceded by a 13 day gap (Fig. 1). As a result of this one measurement and the series of interpolated points preceding it, any emission line light curve calculated from this continuum light curve rises toward the end of the monitoring period. On the other hand, the observed emission line light curves continue to decline to the end. Rather than tamper with the data (we have no *a priori* reason to suspect this measurement), we simply exclude the last 20 days from our fitting procedure to avoid their detrimental effect on the overall fit of the models to the data.

We run a grid of models with $R_{in}$ ranging from 1 to 10 lt-days and $R_{out}$ in the range of 10–70 lt-days. We do this for five choices of differential covering factor dependence on radius: $\alpha = -2, -1, 0, 1, 2$, and four choices of geometry: spherical, and thin disks with axis inclined at an angle $i = 5°$, 45°, and 85°. The resolution of the grid is 1 lt-day in $R_{in}$ for all models, 1 lt-day in $R_{out}$ for the spherical models, and 2 lt-days in $R_{out}$ for the disk models. We therefore calculate a total of 7700 models.

Figure 9 shows the parameter space we investigate. Each frame shows the $R_{in}$-$R_{out}$ projection of parameter space for a certain combination of geometry and $\alpha$. The best-fit model in terms of $R_{in}$ and $R_{out}$ for that combination is marked with a cross and its $\chi^2$ per degree of freedom, $\chi^2_r$, indicated. Several contours of equal $\chi^2_r$ are marked; the innermost is of $\chi^2_r = 1$, the next with $\chi^2_r = 1.19$ (models which can be excluded at the 68% significance level), and the outermost (*thick line*) with $\chi^2_r = 1.52$ (models excluded at the 95% significance level). Note that in some frames the best-fit point has a high $\chi^2_r$ value, so that some of the contours do not exist.

The $\chi^2_r$ values for the best-fitting models show that, for most combinations of geometry and differential covering factor, the models fit the data well (i.e., they cannot be significantly excluded). Comparison of the best-fit $\chi^2_r$ values shows the data are best modeled with spherical or edge-on disk geometries with $\alpha$ of 0 or less. Acceptable models exist for most of the other geometries but are confined to smaller ranges of $R_{in}$ and $R_{out}$. The best-fitting models never occur in the upper right-

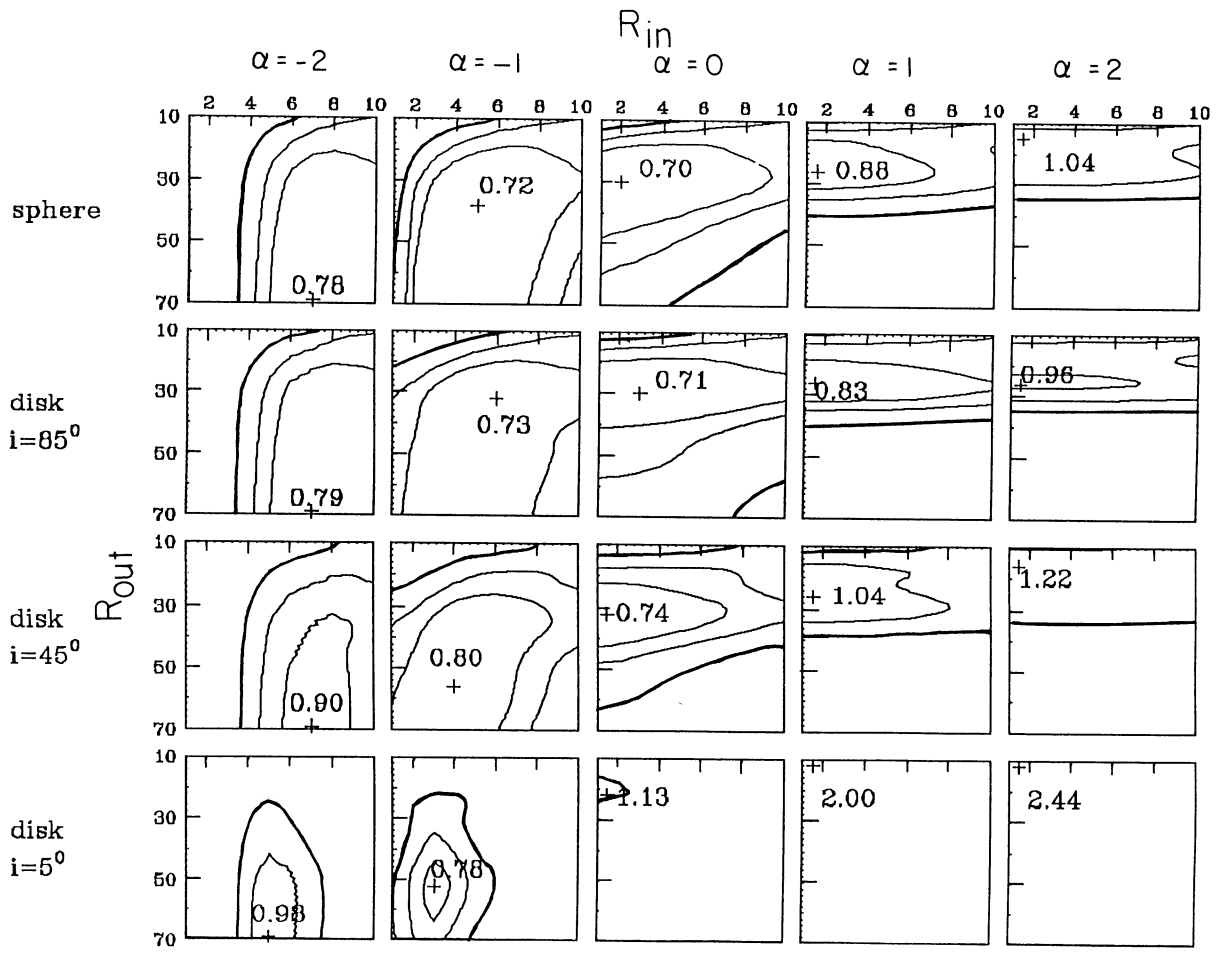


FIG. 9.—Parameter space for the BLR of NGC 4151. Each frame corresponds to a combination of geometry type and emission parameter $\alpha$. Every point inside a frame corresponds to a combination of inner radius $R_{in}$ and outer radius $R_{out}$, indicated in units of lt-days. Best-fit models for each geometry-$\alpha$ combination are marked with a cross and their $\chi^2_r$ value marked. Several contours of equal $\chi^2_r$ are marked; the innermost is of $\chi^2_r = 1$, the next with $\chi^2_r = 1.19$ (models which can be excluded at the 68% significance level), and the outermost (*thick line*) with $\chi^2_r = 1.52$ (models excluded at the 95% significance level). Note that in some frames the best-fit point has a high $\chi^2_r$ value, so that some of the contours do not exist.

hand corners of each frame, corresponding to "thin" ($R_{in} \approx R_{out}$) geometries. The overall best-fit model has a spherical geometry with $\alpha = 0$, $R_{in} = 2$ lt-days, and $R_{out} = 30$ lt-days. Almost exactly as good is an edge-on disk geometry of $\alpha = 0$, $R_{in} = 3$ lt-days, and $R_{out} = 30$ lt-days. Using the "$\Delta\chi^2$" approach, the uncertainty in the best-fit parameters can be estimated. The best-fit inner and outer radii of each geometry and covering factor combination (shown in Fig. 9) and their 68% uncertainty range are listed in Table 2 (this is *not* the range outside of which models can be excluded with 68% confidence, marked by the second contour). Also tabulated for each best-fitting model is $R_{av}$, the emissivity-weighted average radius, defined as

$$R_{av} = \frac{\int_{R_{in}}^{R_{out}} r\, dI(r)}{\int_{R_{in}}^{R_{out}} dI(r)} = \frac{\int_{R_{in}}^{R_{out}} r^{\alpha+1}\, dr}{\int_{R_{in}}^{R_{out}} r^{\alpha}\, dr} .$$

$R_{av}$ is some characteristic BLR radius which can be meaningfully compared to cross-correlation results, or implemented in single-cloud photoionization models (see, e.g., Robinson and Perez 1990). Note in Table 2 that almost all the best-fitting models have $R_{av}$ between 16 and 18 lt-days. The fact that this is a factor of 2 larger than the size derived through cross-correlation (9 lt-days) is not surprising, since all these models are "thick" and therefore would give cross-correlation peaks at lags which are biased toward the inner radius of the BLR (e.g., Maoz and Netzer 1989), namely at about 9 days.

Perhaps more important than the best-fit results, Figure 9 shows there is a large region in geometry-$\alpha$-$R_{in}$-$R_{out}$ space which can be significantly ruled out. In particular, disks with inclinations of 45° or less and $\alpha = 2$, or near face-on disks with $\alpha = 1$ cannot reproduce the observed line variability for any combination of $R_{in}$ and $R_{out}$. Similarly, a large region of the $R_{in}$-$R_{out}$ plane can be excluded for other models with either high $\alpha$ or low inclination.

TABLE 2

BEST-FIT PARAMETERS FOR THE BLR OF NGC 4151

| | $\alpha$ | | | | |
|---|---|---|---|---|---|
| | −2 | −1 | 0 | 1 | 2 |
| | Sphere | | | | |
| $R_{in}$..... | $7^{+2}_{-1}$ | $5^{+2}_{-1}$ | $2^{+3}_{-2}$ | $1^{+4}_{-1}$ | $1^{+7}_{-1}$ |
| $R_{out}$..... | $70_{-34}$ | $38^{+32}_{-9}$ | $30^{+6}_{-4}$ | $26^{+2}_{-3}$ | $15 \pm 2$ |
| $R_{av}$..... | 18 | 16 | 17 | 17 | 11 |
| | Disk ($i = 85°$) | | | | |
| $R_{in}$..... | $7^{+2}_{-1}$ | $6 \pm 2$ | $3 \pm 3$ | $1^{+5}_{-1}$ | $1^{+8}_{-1}$ |
| $R_{out}$..... | $70_{-40}$ | $32^{+8}_{-6}$ | $30 \pm 4$ | $26 \pm 3$ | $26 \pm 3$ |
| $R_{av}$..... | 18 | 16 | 17 | 17 | 20 |
| | Disk ($i = 45°$) | | | | |
| $R_{in}$..... | $7 \pm 2$ | $4 \pm 2$ | $1^{+2}_{-1}$ | $1^{+4}_{-1}$ | $1^{+6}_{-1}$ |
| $R_{out}$..... | $70_{-30}$ | $56_{-24}$ | $32 \pm 4$ | $26 \pm 4$ | $16 \pm 4$ |
| $R_{av}$..... | 18 | 19 | 17 | 17 | 12 |
| | Disk ($i = 5°$) | | | | |
| $R_{in}$..... | $5 \pm 1$ | $3 \pm 1$ | $1 \pm 1$ | No | No |
| $R_{out}$..... | $70_{-22}$ | $52^{+8}_{-6}$ | $22 \pm 2$ | good | good |
| $R_{av}$..... | 15 | 17 | 12 | fit | fit |

NOTE.—All radii in units of lt-days. The 68% confidence interval for the best-fit radii is given. Only the lower limit is given in cases where the upper limit is not in the range of parameter space investigated.

The $\chi^2_r$ values in Figure 9 were calculated assuming a 3% error for the emission line measurements. As stated in § II, this is probably an overestimate of the error. Indeed, the best-fit $\chi^2_r$ values in Figure 9 seem too low (less than 1), indicating that this could be the case. A less conservative estimate of the errors would raise the best-fit $\chi^2_r$ values, cause all the contours to either shrink or disappear, and allow us to rule out more of the parameter space.

Figure 10 shows the light curve (*solid line*) of the best-fit model, a 2–30 lt-day spherical shell with $\alpha = 0$, superposed on the observed Hα light curve. Also shown, for comparison, is the light curve (*dashed line*) of a marginally acceptable (5% probability) model. The fit is remarkable considering it is obtained from a purely geometrical model, under the most simplifying assumptions, and with almost the simplest geometry that comes to mind for the BLR.

The reader may notice, however, that even the best model in Figure 10 systematically misses the data in the dip preceding the large bump in the light curve, and that it fails to reach the peak of the bump (days 55–90). Similarly, as already mentioned above, it cannot reproduce the decline at the end of the observed light curve. This, however, does not necessarily imply that the model is oversimplified or wrong. It should be remembered that not only are there measurement errors in the data being fitted, but there are measurement and interpolation errors in the continuum data used to construct the model light curves as well. To illustrate this point, we show in Figure 11*a* a model continuum light curve obtained by linearly interpolating the observed continuum light curve, except that four out of the 55 measurements are taken 1 $\sigma$ away from their observed values, and one measurement (the problematic one on day 201) is taken 3 $\sigma$ away from its observed value. The emission-line light curve calculated from this continuum light curve, using the same model as in Figure 10, is shown in Figure 11*b*, this time for the whole time span of the data. The fit is considerably improved by these minor modifications, and even the decline in the end is fairly well reproduced.

To summarize, the observed emission line light curve of NGC 4151 can best be modeled by means of a spherical or highly inclined disk-shaped BLR, with a constant or decreasing gradient of the covering factor, and a ratio of outer to inner radius of order 10. BLRs consisting of low-inclination disks, with positive covering factor gradients can be significantly ruled out for a large range of inner and outer radii. We also see

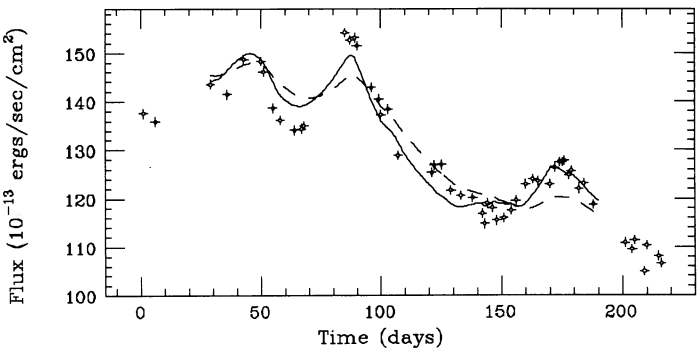


FIG. 10.—The light curve (*solid line*) of the best-fit model found in Fig. 9 (a spherical shell with $R_{in} = 2$ lt-days, $R_{out} = 30$ lt-days, and $\alpha = 0$), superposed on the observed Hα light curve. Also shown, for comparison, is the light curve (*dashed line*) of a marginally acceptable (5% probability) model. Error bars on the data are not shown for clarity's sake.

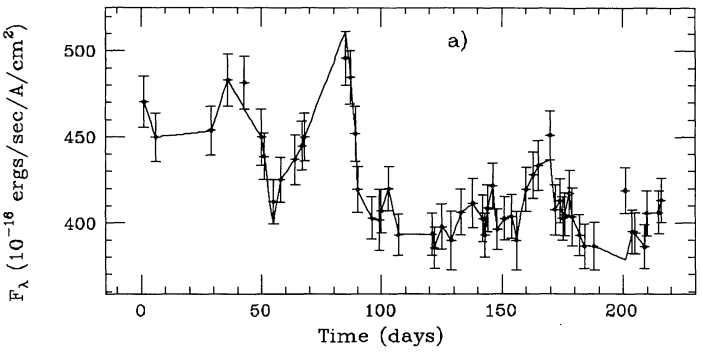


FIG. 11*a*

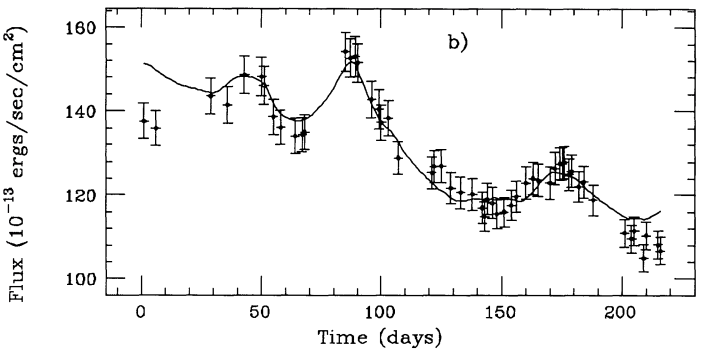


FIG. 11*b*

FIG. 11.—(*a*) A model continuum light curve obtained by linearly interpolating the observed continuum light curve, except that four out of the 55 measurements are taken 1 $\sigma$ away from their observed values and one measurement (on day 201) is taken 3 $\sigma$ away from its observed value. (*b*) The emission line light curve calculated from this continuum light curve, using the same model as in Fig. 10.

that the modeling gives results consistent with those estimated from the deconvolved transfer function, in terms of the general type of geometry. In terms of the BLR dimensions, the model fitting, which is restricted to simple geometries, gives $R_{av} \approx 17$ lt-days. This can be compared to the maximum entropy deconvolution result, which can allow for more complex geometries, and suggests a two-component geometry: an inner component with $R_{out} \approx 15$ lt-days and an extended outer component.

### *e) Measurement of the Velocity Field Asymmetry*

The S/N in the Balmer lines, especially H$\alpha$, is high enough to attempt to measure separately the temporal behavior of the blue and red wings. This can give important clues regarding the velocity field of NGC 4151. To measure H$\beta$, the spectra were aligned in wavelength using the [O III] $\lambda$5007 line. The blue wing was integrated from 4795 to 4857 Å, and the red wing from 4857 to 4930 Å. The continuum was set as before. For the H$\alpha$ measurement the spectra were aligned using the narrow component peak. Using the [O I] $\lambda$6300 line for alignment gave similar results. The blue wing was integrated from 6410 to 6559 Å and the red wing from 6559 to 6670 Å. Spectra which were suspected, based on profile appearance and observation log, of poor guiding or focusing were excluded from this measurement. This left 48 data points for each line, the dates of which are listed in Table 1.

To estimate the additional error introduced in these measurements due to alignment, guiding, and seeing, we experimented in artificially broadening a line profile by convolving it with a Gaussian to a degree that it would appear marginally acceptable, and then shifting it in wavelength by the maximum amount after which it still seemed reasonably aligned. From these experiments, we estimate that, owing mainly to the strength of [O III] and the H$\alpha$ narrow peak, the alignment is accurate to better than 0.2 pixel, or 1 Å. Comparisons of the blue/red fluxes before and after this operation lead to an estimate of the error in the wing fluxes of 5% for both H$\alpha$ and H$\beta$. Note that this error is in addition to the nominal 3% calibration error in each of these fluxes. The errors in the blue and red wing measurements are anticorrelated in a given spectrum, since "misplaced" flux from one wing will unavoidably show up on the other wing.

The results of these measurements are presented in Table 1 and in Figure 12. The H$\alpha$ blue and red wings appear to mimic each other, and the total H$\alpha$ flux, precisely. This is confirmed by the cross correlation function of the two wings, shown as a solid line in Figure 13, which has a very high peak (0.95) at a lag of $-1$ day (in other words, the blue wing lags the red wing by one day). As we will show below, this small deviation from zero could easily be caused by the anticorrelation in the errors mentioned above. The data indicate, therefore, that the blue and red wings of H$\alpha$ vary almost completely in phase. The H$\beta$ measurement is predictably noisy due to the statistical noise in a signal now only half the strength of the already weak signal in the total flux measurement. Nonetheless, here too the light curves of the two wings appear very similar. Their cross-correlation (Fig. 13, *dashed line*) has a peak of 0.84 at a lag of $-5$ days (the blue wing lags the red by 5 days).

To investigate the implications of these results for models of radial motion in the BLR, we carry out Monte-Carlo simulations similar to those of § III*a*. The observed continuum light

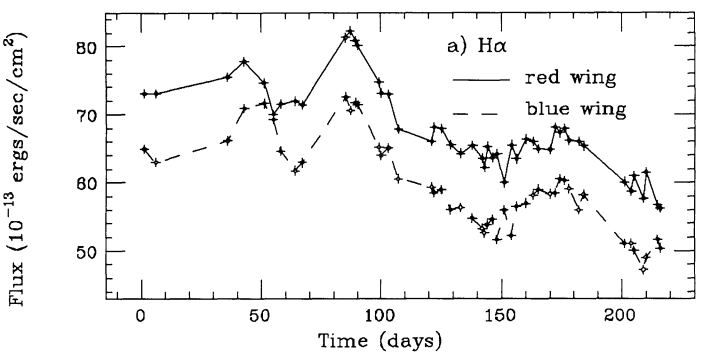


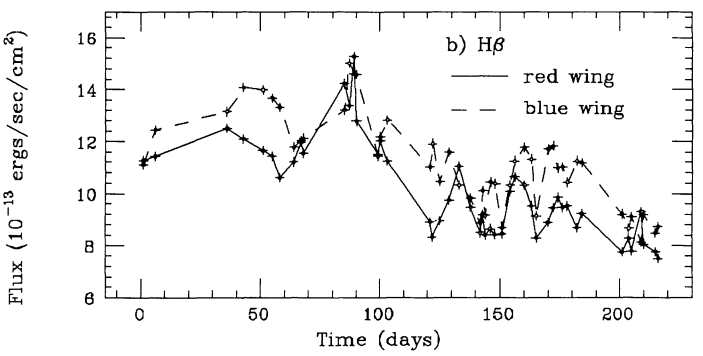


FIG. 12.—Light curves of the blue and red wing fluxes as measured separately. (*a*) H$\alpha$. (*b*) H$\beta$.

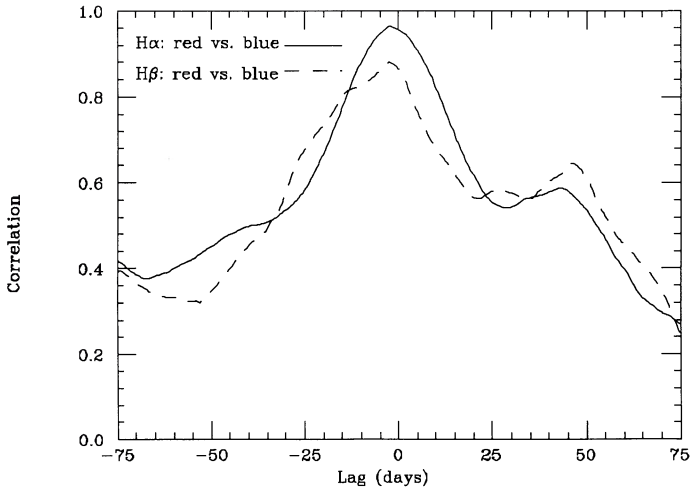


FIG. 13.—Cross-correlation functions of the red wing vs. the blue wing flux for Hα (*solid line*) and Hβ (*dashed line*).

curve is convolved with the transfer functions of the near and far halves of a shell of inner radius 2 lt-days and outer radius 30 lt-days, with $\alpha = 0$. (This was the best-fit model found in § III*d*, above.) The two calculated light curves, shown in Figure 14*a*, correspond to the blue and red wings of a line in a pure inflow or outflow model. Note that for such "thick" spherical shells, the "near" and "far" wing light curves are quite different, rather than being similar and simply shifted in time with respect to each other. This is because the transfer function of the near hemisphere is nonzero between $t = 0$ and $t = R_{out}/c = 30$ days, while that of the far hemisphere is nonzero between $t = R_{in}/c = 2$ days and $t = 2R_{out}/c = 60$ days. So, in effect, the response of the far hemisphere is spread over a time almost twice as long, making it much less coherent. The shapes of the transfer functions are also different, that of the far hemisphere being more weighted toward larger lags compared to that of the near side.

To find the probability distribution of the cross-correlation peak, the two calculated light curves are sampled at random at 48 points, the *same* 3% random measuring error added to both at each point, and an *opposite* 5% error added to each. The resulting light curves are cross-correlated, and the peak of the cross-correlation found and noted. The process is repeated 1000 times to derive the probability of obtaining the observed −1 day and −5 day lags between the red and blue wings, assuming this type of pure inflow or outflow model. Figure 14*b* shows the empirical probability distribution (or CCPD; see Maoz and Netzer 1989) obtained this way. The CCPD shows that the most probable lag between the line wings emitted from the near and far hemispheres of such a model is around 11 days. Under our assumed errors and sampling rate, the probability of observing a lag of 5 days or less between the wings is 3.3%. *Both the* Hα *and the* Hβ *results therefore rule out radial flow in the BLR of NGC 4151.* We have repeated this calculation for the case of a more steeply declining covering factor gradient, of $\alpha = -2$. In such a case the above conclusions are only strengthened, since $R_{av}$ becomes smaller, the response of the wings more coherent, and the CCPD narrower. These results contradict the claim made by Gaskell (1988) that radial inflow plays a significant role in the velocity field of the inner BLR in NGC 4151.

If we have seriously underestimated our errors, the CCPD could broaden somewhat, so that the probability of obtaining a lag of 5 days or less would exceed 5%. The Hβ result alone would then not rule out significantly pure inflow of the gas. The probability of observing a lag of 1 day or less is only 0.5% so that the ruling out of radial flow of the Hα emitting gas is quite robust even if we have seriously underestimated the errors. The great similarity of the total-flux Hα and Hβ light curves (Figs. 1*b*, 1*c*, and 2*b*) suggests that the gases emitting them share a common geometry. It would be implausible that the gas emitting each line does not then share the same velocity field as well. Finally, the wing measurements of both lines are fully consistent with a situation in which the two wings of each line are varying completely in phase: We have repeated the Mont-Carlo simulation for a model in which both wings vary identically according to the response of a 2–30 lt-day thick shell of $\alpha = 0$. Under this hypothesis, there is a 20% probability of obtaining a lag of 5 days or more. Only an observed lag greater than 8 days would contradict this model. In such a

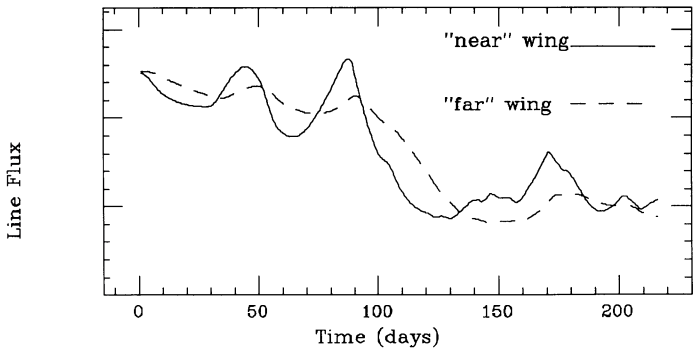


FIG. 14*a*

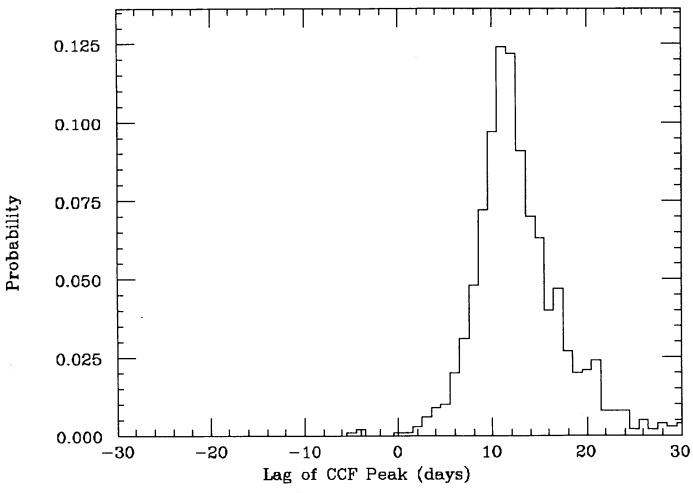


FIG. 14*b*

FIG. 14.—(*a*) Light curves calculated by convolving the linearly interpolated observed continuum light curve with the transfer functions of the near (*solid line*) and far (*dashed line*) hemispheres of a shell of inner radius 2 lt-days and outer radius 30 lt-days, with $\alpha = 0$. Such light curves would arise for the two wings of a line in a model with such a geometry having pure radial flow. (*b*) The cross-correlation peak distribution (CCPD) obtained by sampling at random the above light curves in a Monte-Carlo process (see text for details). It shows the probability of obtaining a certain lag of the peak of the cross-correlation function for the two wings, assuming this type of model.

model, the 68% probability range is $0 \pm 5$ days. This can be considered to be the range to within which we have determined that the wings of the Balmer lines in NGC 4151 vary in phase.

## IV. DISCUSSION AND CONCLUSIONS

In the previous section, we analyzed the data for NGC 4151 according to the following procedure.

1. The lag between the lines and the continuum was found through cross-correlation, and Monte Carlo simulations were used to find the constraints imposed by the lag on BLR models.

2. Fourier and maximum entropy deconvolutions were used to recover the BLR transfer function, from which the BLR parameters were estimated.

3. The observed continuum light curve was convolved with a grid of transfer functions corresponding to simple BLR geometries in an attempt to find the best-fit parameters of the BLR and the regions of parameter space which can be significantly excluded by the data.

4. The velocity field of the BLR was studied by cross-correlating the blue and red wings of the lines and again using Monte Carlo simulations to find constraints on the models. In this section we briefly discuss the results of this analysis in the light of current concepts regarding AGNs.

The "standard" photoionization model of AGNs (e.g., Davidson and Netzer 1979) required BLR gas in AGNs of all luminosities to have an ionization parameter (defined as the ratio of ionizing photon density to electron density) in a small range around a value of order 0.01. This implied that in AGNs of different luminosities, the line-emitting gas is somehow always at a distance from the source such that it has the same ionization parameter, or in other words, that the size of the BLR scales as the square root of the luminosity. The model also predicted this size to be of order light-months for Seyfert galaxies and light-years for quasars. Variability studies carried out during the past decade in order to test this prediction indicated, for a number of AGNs, BLR sizes one to two orders of magnitude smaller (see Peterson 1988 for a review). However, as the spacing of the observations was planned according to the model predictions, the data turned out to be temporally undersampled, and the BLR size could not be measured accurately. Our AGN monitoring program was designed to be able to discern the small lags, of order a week, indicated by the previous studies and thus allow an accurate determination of the BLR size.

The $9 \pm 2$ day lag between the Balmer lines and the continuum measured by our observations constitutes the third (after Mrk 279 and NGC 5548) such accurate measurement for an AGN. It is the first accurate measurement in NGC 4151, where, as described in § I, previous estimates ranged from 2 to 20 days. This result is surprising since it is very similar to, and even slightly larger than, the lag of 7 days found for NGC 5548, an object about 10 times more luminous. This makes its BLR size intermediate between the predictions of "old" photoionization models and of new, high-ionization parameter models calculated to explain the small observed BLR sizes of other AGNs (Netzer 1989; Ferland and Persson 1989). The unusually small discrepancy of NGC 4151 with the old models has been noted before (e.g., Peterson 1988; Maoz and Netzer 1989) and is now confirmed. In fact, an "intermediate" ionization parameter ($\log U = -0.75$) model of Ferland and Mushotzky (1982) tailored specifically to account for the observed UV/optical spectrum of NGC 4151 predicted a BLR radius of 15 lt-days, in excellent agreement with the 16–18 lt-day emissivity-weighted radius we have found from model fitting; one could argue then that here is at least one Seyfert galaxy where there is *no* discrepancy between the old theory and the observations. This is under the now questionable assumption that AGNs of all luminosities have the same ionization parameter. This assumption can be tested when the BLR size of more objects becomes known and it can be seen whether it scales as the square root of the luminosity. A more meaningful comparison should be made to a photoionization model implementing the geometric structure of the BLR, as reflected in this work.

We can conjecture several possible causes for the relatively large size observed. If NGC 4151 is 5–10 times more luminous than it appears to us due to, e.g., obscuration (e.g., Miller 1989) or the effect of an accreton disk supplying the UV continuum radiation being viewed edge on (Netzer 1987), then it would be similar to other AGNs. Similarly, NGC 4151 may on the average have a higher luminosity, which determines the BLR size, while we are now seeing it at a low phase. Alternatively, NGC 4151 may be part of a separate, low-ionization parameter class of AGNs. There is circumstantial evidence for each of these arguments. For example, Pogge (1989), Perez *et al.* (1989), and Perez-Fournon and Wilson (1990) analyzed high-resolution images of the extended narrow-line region of this galaxy. An obscuring band may exist on the nucleus, lying perpendicular to the elongated high-ionization region. These studies favor an interpretation of the elongated structure as resulting from the collimation of ionizing radiation emitted by the nucleus, while Penston *et al.* (1990) show that the beam is constrained to be very close to the plane of the sky. Ulrich *et al.* (1985) and Clavel *et al.* (1987) also speculate that the unidentified satellite lines of C IV $\lambda$1549 arise in a two-sided jet lying close to the plane of the sky. A combination of dust torus, accretion disk, and perhaps disk-shaped BLR, all coaxial and viewed edge-on, would support the first scenario suggested above. In support of the second scenario, NGC 415 is not a prototype Seyfert 1; in its low states it could perhaps be better classified as a Seyfert 2 (Penston and Perez 1984). Perhaps such objects which fluctuate between states are a separate class.

Our finding that H$\alpha$ and H$\beta$ vary with the same lag after the continuum contradicts Gaskell and Sparke's (1986) claim that the higher the order of the Balmer lines, the smaller the lag, and in particular, that H$\alpha$ lags H$\beta$ by $\sim$13 days. Our data imply that these two Balmer lines are emitted in the same region. The Balmer decrement is thus independent of distance from the center. Any reddening that is present is the same for the whole BLR.

Our investigation of the BLR geometry and velocity field affords a first look inside the region and considerably limits the range of possible models. The constraints we have found on the geometry should be useful in building future models for this object. The fitting of the observed emission line light curve shows that it is best reproduced by thick, spherical or preferably edge-on disk, BLR models with $-2 \leq \alpha \leq 0$. These types of geometry are also indicated by the transfer function recovered through maximum entropy deconvolution.

Until now, the only constraint on $\alpha$ had come from the velocity profile of the emission lines, after assuming a certain velocity field (e.g., Scoville and Norman 1988). For instance, assuming a Keplerian dependence of velocity on distance from the center, $v(r) \propto r^{-1/2}$, then (for a spherical geometry) $\alpha = -3/2$ is needed to reproduce the approximately logarithmic observed line profiles. Our observations favor a slowly

decreasing gradient of the covering factor, regardless of the velocity's radial dependence. Such a radial dependence of the covering factor is in fact predicted by several physical models. For example, Rees, Netzer, and Ferland (1989) study situations relevant for clouds with a size controlled by a pressure law, that would give $\alpha$ between $-\frac{1}{2}$ and $-\frac{1}{6}$; Bahcall and Woolf (1976) showed that the number density of stars in a cluster dominated by a central black hole is $N(r) \propto r^{-7/4}$. Scoville and Norman (1988) and Kazanas (1989) use this distribution in models in which the BLR–emitting objects are the irradiated atmospheres of stars in a central cluster. Since $dC(r) = N(r)\sigma(r)dr$, the requirement of small negative $\alpha$ means that the cross-sectional area $\sigma(r)$ of the stellar atmospheres should not increase too fast with distance of the star from the cluster center. For this $N(r)$, the same requirement arises from the line profile, as mentioned above.

Perhaps our most important result is the ruling out of pure, unidirectional radial motion of the Balmer line–emitting gas. Radial inflow or outflow has often been invoked in AGN models (e.g., Capriotti, Foltz, and Byard 1981; Mathews and Capriotti 1984). Our result eliminates the problem of an asymmetric Ly$\alpha$ profile predicted by such motion, in conflict with the observed symmetric profile (Wilkes and Carswell 1982).

We have shown in practice the wealth of information about an AGN that can be derived through a study of its variability. Future studies should strive to increase even further the sampling rate in order to measure better the transfer function and thus uniquely determine the geometry of the BLR. Serious efforts should be made to do this with a high spectral resolution that will also reveal clearly the form of the velocity distribution. This could enable the first direct probing of the gravitational field very close to the "central engine." NGC 4151, with its large apparent brightness, is an excellent candidate for such future work.

We thank Ezra Mashal and Sammy Ben-Guigui, of the Wise Observatory staff, for their dedicated assistance with the observations. This work has benefited from comments by John Bahcall, Rick Edelson, Brad Peterson, and Mike Shull. Bill Welsh, Dan Lester, and Ramesh Narayan are thanked for suggesting the use of maximum entropy and for tips on the method. We thank the referee for several helpful comments and suggestions. This work was supported by grant 85/00085 from the United States-Israel Binational Foundation, Jerusalem, Israel, and by grants from the Israel Academy of Sciences and the Israeli Ministry of Science and Development.

## REFERENCES

Antonucci, R. R. J., and Cohen, R. D. 1983, *Ap. J.*, **271**, 564.
Bahcall, J. N., and Woolf, R. A. 1976, *Ap. J.*, **209**, 214.
Blandford, R. D., and McKee, C. F. 1982, *Ap. J.*, **255**, 419.
Boksenberg, A., Shortridge, K., Allen, D. A., Fosbury, R. A. E., Penston, M. V., and Savage, A. 1975, *M.N.R.A.S.*, **173**, 381.
Capriotti, E., Foltz, C., and Byard, P. 1980, *Ap. J.*, **241**, 903.
Clavel, J., *et al.* 1987, *Ap. J.*, **321**, 251.
Clavel, J., *et al.* 1990, *Ap. J.*, in press.
Clavel, J., *et al.* 1991, *M.N.R.A.S.*, in press.
Davidson, K., and Netzer, H. 1979, *Rev. Mod. Phys.*, **51**, 715.
Edelson, R. A., and Krolik, J. H. 1988, *Ap. J.*, **333**, 646.
Ferland, G. J., and Mushotzky, R. F. 1982, *Ap. J.*, **262**, 564.
Ferland, G. J., and Persson, S. E. 1989, *Ap. J.*, **347**, 656.
Gaskell, C. M. 1988, *Ap. J.*, **325**, 114.
Gaskell, C. M., and Sparke, L. S. 1986, *Ap. J.*, **305**, 175.
Kazanas, D. 1989, *Ap. J.*, **347**, 74.
Lester, D. F., Harvey, P. M., and Joy, M. 1986, *Ap. J.*, **302**, 280.
Malkan, M. A., and Filippenko, A. V. 1983, *Ap. J.*, **275**, 477.
Maoz, D., and Netzer, H. 1989, *M.N.R.A.S.*, **236**, 21.
Maoz, D., *et al.* 1990, *Ap. J.*, **351**, 75 (Paper I).
Mathews, W. G., and Capriotti, E. R. 1985, in *Astrophysics of Active Galaxies and Quasi-Stellar Objects*, ed. J. S. Miller (Mill Valley: University Science Books), p. 185.
Miller, J. S. 1989, in *Active Galactic Nuclei*, ed. D. E. Osterbrock and J. S. Miller (Dordrecht: Kluwer), p. 273.
Narayan, R., and Nityananda, R. 1986, *Ann. Rev. Astr. Ap.*, **24**, 127.
Netzer, H. 1987, *M.N.R.A.S.*, **225**, 55.
———. 1989, *Comments Ap.*, **14**, 137.
Netzer, H., *et al.* 1990, *Ap. J.*, **353**, 108 (Paper II).
Penston, M. V., Penston, M. J., and Sandage, A. 1971, *Pub A.S.P.*, **83**, 783.
Penston, M. V., and Perez, E. 1984, *M.N.R.A.S.*, **211**, 33P.
Penston, M. V., *et al.* 1990, *Astr. Ap.*, **236**, 53.
Perez, E., Gonzales-Delgado, R., Tadhunter, C., and Tsevatanov, Z. 1989, *M.N.R.A.S.*, **241**, 31P.
Perez-Fournon, I., and Wilson, A. S. 1990, *Ap. J.*, in press.
Peterson, B. M. 1988, *Pub. A.S.P.*, **100**, 18.
Peterson, B. M., and Cota, S. A. 1988, *Ap. J.*, **330**, 111.
Pogge, R. W. 1989, *Ap. J.*, **345**, 730.
Press, W. H., Flannery, B. P., Teukolsky, S. A., and Vetterling, W. T. 1986, *Numerical Recipes* (Cambridge: Cambridge University Press).
Rees, M. J., Netzer, H., and Ferland, G. J. 1989, *Ap. J.*, **347**, 640.
Robinson, A., and Perez, E. 1990, *M.N.R.A.S.*, **244**, 138.
Scoville, N., and Norman, C. 1988, *Ap. J.*, **332**, 163.
Solomos, N., Whitehead, M. J., Meaburn, J., Goudis, C. D., and Christopoulou, P. E. 1990, *Astr. Ap.*, **229**, 80.
Ulrich, M. H., *et al.* 1984, *M.N.R.A.S.*, **206**, 221.
Ulrich, M. H., *et al.* 1985, *Nature*, **313**, 745.
Wilkes, B. J., and Carswell, R. F. 1982, *M.N.R.A.S.*, **201**, 645.
Willingale, R. 1981, *M.N.RA.S.*, **194**, 359.

ELHANAN ALMOZNINO, SARA BECK, NOAH BROSCH, ELIA LEIBOWITZ, TSEVI MAZEH, HAIM MENDELSON, and HAGAI NETZER: School of Physics and Astronomy, Tel-Aviv University, Tel-Aviv 69978, Israel

ARI LAOR and DAN MAOZ: The Institute for Advanced Study, Princeton, NJ 08540